Observation of an MHD Alfvén vortex in the slow solar wind

Roberts, Owen; Li, Xing; Alexandrova, O.; Li, Bo

Published in:
Journal of Geophysical Research

DOI:
10.1002/2015JA022248

Publication date:
2016

Citation for published version (APA):
Roberts, O., Li, X., Alexandrova, O., & Li, B. (2016). Observation of an MHD Alfvén vortex in the slow solar wind. *Journal of Geophysical Research*, *121*(5), 3870-3881. https://doi.org/10.1002/2015JA022248

AGU PUBLICATIONS

JGR

Journal of Geophysical Research: Space Physics

RESEARCH ARTICLE

10.1002/2015JA022248

Special Section:
Nature of Turbulence, Dissipation, and Heating in Space Plasmas: From Alfven Waves to Kinetic Alfven Waves

Key Points:
- Fluctuations have low speed in the plasma frame indicative of an advected structure or a slowly propagating wave
- Comparison of data with an Alfvén vortex model shows excellent agreement
- Polarization of the fluctuations is consistent with a vortex structure

Correspondence to:
O. W. Roberts,
Owen.Roberts@esa.int

Citation:
Roberts, O. W., X. Li, O. Alexandrova, and B. Li (2016), Observation of an MHD Alfvén vortex in the slow solar wind, *J. Geophys. Res. Space Physics*, *121*, 3870–3881, doi:10.1002/2015JA022248.

Received 7 DEC 2015
Accepted 8 APR 2016
Accepted article online 18 APR 2016
Published online 5 MAY 2016

Observation of an MHD Alfvén vortex in the slow solar wind

O. W. Roberts[1,2], X. Li[2], O. Alexandrova[3], and B. Li[4]

[1]SCI - S ESTEC/ESA, Keplerlaan 1, Noordwijk, Netherlands, [2]Department of Physics, Aberystwyth University, Aberystwyth, UK, [3]LESIA, Observatoire de Paris, PSL Research University, CNRS, Sorbonne Universités, UPMC Univ. Paris 06, Université Paris Diderot, Sorbonne Paris Cité, France, [4]Shandong Provincial Key Laboratory of Optical Astronomy and Solar-Terrestrial Environment, Institute of Space Sciences, Shandong University, Weihai, China

Abstract In the solar wind, magnetic field power spectra usually show several power laws. In this paper, magnetic field data from the Cluster mission during an undisturbed interval of slow solar wind are analyzed at 0.28 Hz, near the spectral break point between the ion inertial and dissipation/dispersion ranges. Assuming Taylor's frozen-in condition, it corresponds to a proton kinetic scale of $kv_A/\Omega_p \sim 0.38$, where v_A and Ω_p are the Alfvén speed and proton angular gyrofrequency, respectively. Data show that the Cluster spacecraft passed through a series of wave packets. A strong isolated wave packet is found to be in accordance with the four Cluster satellites crossing an Alfvén vortex, a nonlinear solution to the incompressible MHD equations. A strong agreement is seen between the data from four satellites and a model vortex with a radius of the order of 40 times the local proton gyroradii. The polarization at different spacecraft is compared and is found to agree with the vortex model, whereas it cannot be explained solely by the linear plane wave approach.

1. Introduction

In neutral fluids, turbulence yields eddies from large to ever smaller scales until the turbulent energy is eventually dissipated by viscosity. In plasmas, the magnetic field brings complications so that not only eddies but waves and current sheets are also commonplace, and all these contribute to the dissipation of the turbulence power. Kinetic effects make studying the turbulence more challenging at ion and electron kinetic scales.

The solar wind is one of the best natural laboratories to study the plasma turbulence [*Tu and Marsch*, 1995; *Bruno and Carbone*, 2013]. The existence of a magnetic field makes the solar wind turbulence highly anisotropic with $k_\perp \gg k_\parallel$ [*Shebalin et al.*, 1983; *Bieber et al.*, 1996; *Goldreich and Sridhar*, 1995], where $k_\perp$ and $k_\parallel$ represent wave numbers along directions perpendicular and parallel to the mean magnetic field, respectively. This anisotropy tends to be true at both MHD and ion kinetic scales [*Horbury et al.*, 2008; *Podesta*, 2009; *Wicks et al.*, 2010; *Chen et al.*, 2010; *Sahraoui et al.*, 2010; *Narita et al.*, 2011; *Roberts et al.*, 2013; *Roberts*, 2014; *Roberts et al.*, 2015]. A typical magnetic field turbulent power spectrum involves an energy injection scale with a scaling of k^{-1} for low wave numbers, where Alfvénic turbulence dominates and energy is deposited into the system. At intermediate wave numbers, an ion inertial range with a $k^{-5/3}$ Kolmogorov scaling is present until reaching a spectral break at ion scales ($k\rho_i \sim 1$ or $kd_i \sim 1$, where ρ_i and d_i are the proton Larmor and inertial lengths, respectively). The spectrum steepens beyond this spectral break [*Leamon et al.*, 1998; *Smith et al.*, 2001, 2006; *Hamilton et al.*, 2008]. At scales smaller than ion scales and up to electron scales, the spectrum follows a scaling of around −2.8 [*Alexandrova et al.*, 2009; *Sahraoui et al.*, 2010; *Alexandrova et al.*, 2012]. At MHD scales, turbulence is dominated by Alfvénic fluctuations [*Belcher*, 1971].

The nature of solar wind turbulence is still an open question: can waves still be used to describe turbulence (as a first approximation), or is it necessary to adopt the strong turbulence paradigm? To understand turbulent heating in space plasmas, it is essential to understand the different contributions of these different phenomena to the overall energy budget. Dissipation in relation to waves may come from Landau damping or cyclotron resonance, while for coherent structures the possible mechanisms are reconnection or currents. Simulations by *Karimabadi et al.* [2013] and observations by *Roberts et al.* [2013] suggest that coherent structures and waves may coexist in the solar wind. Therefore, understanding which paradigm best describes the observed fluctuations has relevance for not only dissipative heating but also the turbulent cascade itself. Some properties of turbulence fluctuations such as magnetic helicity and dispersion plots have often been interpreted in the wave paradigm as being due to kinetic Alfvén waves (KAWs) or a mixture of KAWs and ion cyclotron waves [*He et al.*, 2011; *Roberts and Li*, 2015]. Strong turbulence may be dominated by nonlinear coherent structures such as current sheets [*Siscoe et al.*, 1968; *Vasquez et al.*, 2007], magnetic vortices like the Orszag-Tang vortex [*Orszag and Tang*, 1979], or Alfvén vortices of the MHD type [*Petviashvili and Pokhotelov*, 1985, 1992], drift type *Shukla et al.* [1985], or kinetic type *Shukla et al.* [1985a]. In a broader context, some detailed observations of coherent vortices are available in the Earth's and Saturn's magnetic environments. Observational evidence of drift vortices in the Earth's ionosphere can be found in *Chmyrev et al.* [1988] and *Volwerk et al.* [1996]. Large-scale Kelvin-Helmholtz vortices have been observed on the Earth's magnetopause [*Hasegawa et al.*, 2004]. Kinetic Alfvén vortices were identified with multipoint Cluster measurements in the magnetospheric cusp region [*Sundkvist et al.*, 2005; *Sundkvist and Bale*, 2008]. While the first observational evidence of MHD Alfvén vortices in space plasmas was presented in *Alexandrova et al.* [2006], where a multipoint analysis with Cluster clearly shows the topology of these magnetic structures and their propagation in the plasma frame. While these observations were made in the Earth's magnetosheath, *Alexandrova and Saur* [2008] showed the existence of such structures in the magnetosheath of Saturn. Regarding the solar wind, the only published signatures of vortex structures were presented by *Verkhoglyadova et al.* [2003] using single-satellite measurements, where a particular kind of polarization and discontinuities in the solar wind were explained with an Alfvén vortex model. More recently, a study by *Lion et al.* [2016] shows the presence of Alfvén vortex-like structures in the fast solar wind as measured with the Wind spacecraft. These structures occur close to ion characteristic scales, similar to what happens to the vortices observed in the Earth's magnetosheath [*Alexandrova et al.*, 2006].

The studies of *Alexandrova and Saur* [2008] and *Lion et al.* [2016] both employed single-point measurements. As such, they cannot definitively demonstrate the spatial localization of Alfvén vortices. A multisatellite analysis is needed. A recent statistical study of coherent structures around ion scales by D. Perrone et al. Compressive coherent structures at ion scales in the slow solar wind, submitted to *Plasma Physics*, 2016, arXiv:1604.07577[physics.plasm - ph] shows the presence of Alfvén vortex-like structures in a compressible slow wind stream. These structures have $k \perp$ to $\mathbf{B_0}$ and slow propagation in the plasma rest frame, which was possible to estimate with four Cluster spacecraft. The space localization is verified, but the fluctuations have not been compared to the vortex model on four satellites to confirm the interpretation by the Alfvén vortex. In two recent papers by *Roberts et al.* [2013, 2015], a k-filtering analysis based on four satellites' measurements has shown that turbulent fluctuations around ion scales have $k_\perp \gg k_\parallel$ and $\omega \simeq 0$ in the plasma frame. This was interpreted as a mixture of kinetic Alfvén waves (KAWs) and coherent structures such as vortices. *Roberts et al.* [2013] also performed an analysis of the polarization of magnetic field fluctuations in the plane perpendicular to the global background magnetic field $\mathbf{B_0}$. In this plane, several coherent rotations of the magnetic field fluctuations were observed, indicating the presence of coherent structures. Here we reanalyze one of the time intervals examined in *Roberts et al.* [2015] to show that it is possible to identify an Alfvén vortex structure using simultaneous measurements from all four Cluster spacecraft. The end result is that we give clear evidence of the existence of an Alfvén vortex in the solar wind.

2. Data and Methodology

We use the magnetic field data obtained from the Fluxgate Magnetometer instrument (FGM) [*Balogh et al.*, 2001] on the Cluster mission [*Escoubet et al.*, 1997]. A 10 min interval which occurs on 16 February 2005 between 22:30 and 22:40 UT is studied, when the craft was in the slow solar wind. The angle between the magnetic field and the bulk velocity is quite large ($\theta_{\mathbf{vB}} > 60°$), indicating that there is no magnetic connection to the bow shock. The E field spectrogram from the Waves of High frequency and Sounder for Probing of Electron density by Relaxation (WHISPER) [*Décréau et al.*, 2001] instrument is quiet (not shown), with no signatures of high-frequency waves characteristic of the foreshock [*Lacombe et al.*, 1985; *Alexandrova et al.*, 2013]. Some typical plasma parameters obtained from Cluster C1 FGM and the Cluster Ion Spectrometer (CIS) [*Rème et al.*, 2001] are given in Table 1. For this chosen event, the magnetic field is relatively stable and free from obvious discontinuities. The latter is required because discontinuities would give large changes in $\mathbf{B_0}$ and $\delta B_\parallel$, thereby violating the incompressibility assumption of the vortex model. In addition to the low compressibility this interval was also selected since the Cluster spacecraft configuration was close to a regular tetrahedron, and the corresponding spatial scale of the wave packet is larger than the interspacecraft distances ensuring that all spacecraft see the same wave packet. This interval was previously analyzed by *Roberts et al.* [2015], who concluded that the dispersion plot at scales slightly larger than those studied here ($kv_A/\Omega_p \sim 0.3$) was characteristic of either kinetic Alfvén waves or static structures.

Table 1. Spacecraft and Mean Plasma Parameters[a]

v_{sw} (km s^{-1})	B_0 (nT)	v_A (km s^{-1}	n (cm^{-3})	f_{ci} (Hz)	$\theta_{\mathbf{vB}}$ (deg)	$T_{i\perp}/T_{i\parallel}$	ρ_i (km)	d_i (km)	β	d_{min} (km)
377	11.9	85.8	9.2	0.181	112°	0.5	38.4	75.4	0.57	896.8

[a]Here v_{sw} and v_A denote the bulk speed and Alfvén speed, respectively. In addition, B_0 is the magnitude of the magnetic field, n is the number density of protons, f_{ci} is the proton gyration frequency, θ_{vB}(°) is the angle between the magnetic field and the bulk velocity, $T_{i\perp}/T_{i\parallel}$ is the ratio of perpendicular to parallel temperatures of protons, and d_i and ρ_i denote the ion inertial length and Larmor radius, respectively. The plasma beta is denoted by β, and d_{min} represents the minimum distance between a Cluster spacecraft pair.

Figure 1a shows the raw magnetic field data in the Geocentric Solar Ecliptic (GSE) coordinate system from the FGM instrument. One can see that $|\mathbf{B}|$ does not vary much in the interval. Figure 1b shows the magnetic fluctuations defined here as $dB_i = B_i - \langle B_i \rangle_{30s}$ where the time average is done over the 30 s between two vertical lines of Figure 1a. Here one can see coherent, localized in time event in the middle of the time interval, between 5 and 15 s, visible mostly in dB_y (blue) and dB_z (green) components. At around 10.5 s all three fluctuation components are zero, suggesting that the spacecraft pass through a localized current sheet or a current filament at this point. At the end of the interval, there is another event with three components changing in phase. In our study we will focus on the central structure at $t = 10$ s. Figure 1c shows the power spectral density (PSD) of the three magnetic field components and of $|\mathbf{B}|$ for the 10 min time interval shown in Figure 1a. One can see that between 0.2 and 0.3 Hz, there is a local maximum on the PSD($|\mathbf{B}|$) that can be a satellite spin effect (we will discuss this point in more detail below). In the PSD of the components, at the same frequencies one observes a spectral knee. Then, between 0.2 and 1 Hz, the PSD(B_z) (green line) follows a clear power law, which breaks to a steeper scaling of around −2.9 at $f > 1$ Hz . Other magnetic field components arrive to the noise floor at $f > 1$ Hz, so we cannot conclude about the shape of the PSD of B_x and B_y at high frequencies. It appears that the noise floor (where the spectra flatten due to instrumental noise near $f \gtrsim 1.5$ Hz) appears lower in the B_z component compared to B_x and B_y, the components in the satellite spin plane. If it was related only for the spin problem, it would be expected to be similar for all spacecraft, which is not observed for spacecraft C2 and C4 where the noise floor is similar for all three components (not shown).

Figure 2 shows magnetic scalograms calculated with Morlet wavelet transform for three components of magnetic field but in primed coordinates, where $\mathbf{e}_{z'}$ is the unit vector along the background magnetic field $\mathbf{B_0}$; the other two unit vectors are defined as follows:

$$\mathbf{e}_{x'} = [-B_y A/B_x, A, 0], \tag{1}$$

$$\mathbf{e}_{y'} = \mathbf{e}_{z'} \times \mathbf{e}_{x'}, \tag{2}$$

where $A = B_x/\sqrt{B_x^2 + B_y^2}$. This system was chosen such that the velocity vector (predominantly in the $-x$ GSE direction) is mostly in the $+x'$ direction (since the largest component of $\mathbf{B_0}$ is in the negative y (GSE) direction, see Figure 1a). The background magnetic field $\mathbf{B_0}$ used here is the global average for the 10 min interval. It is important to note that the local mean field around the structure shown in Figure 1b and the global mean (the mean for the full 10 min interval) are similar in this time interval.

In the plane perpendicular to $\mathbf{B_0}$ (see Figures 2a and 2b), one observes localized energetic events covering a range of scales, from $\sim$ 1 to $\sim$ 5 s. Exactly at the corresponding frequencies, (0.2,1) Hz, we observe a power law spectrum in Figure 1c, as discussed above. These events have different energies and vary a bit in scales. In case of a technical issue, like spin, it would appear in a scalogram as a constant energy emission at a fixed scale, which is not the case of energetic events observed here. Thus, there is no clear spin effect present in the scalograms, and spectral leakage of any fluctuations due to the spacecraft spin is not likely to affect the magnetic fluctuations of the localized energetic events.

The coherent magnetic fluctuations of Figure 1b correspond to the energetic event between two vertical dotted lines in the scalograms: here the energetic peak appears around 3.6 s timescale. We will study magnetic fluctuations associated with this energetic event around its central scale, between frequencies 0.23 and 0.36 Hz (between the dashed lines in Figures 1c and 2). For this purpose, the data in the primed coordinate system are bandpass filtered using a wavelet transform [*Torrence and Compo*, 1998] and reconstructed as time series [*Roberts et al.*, 2013] such that only signals from this narrow range of frequencies are present.

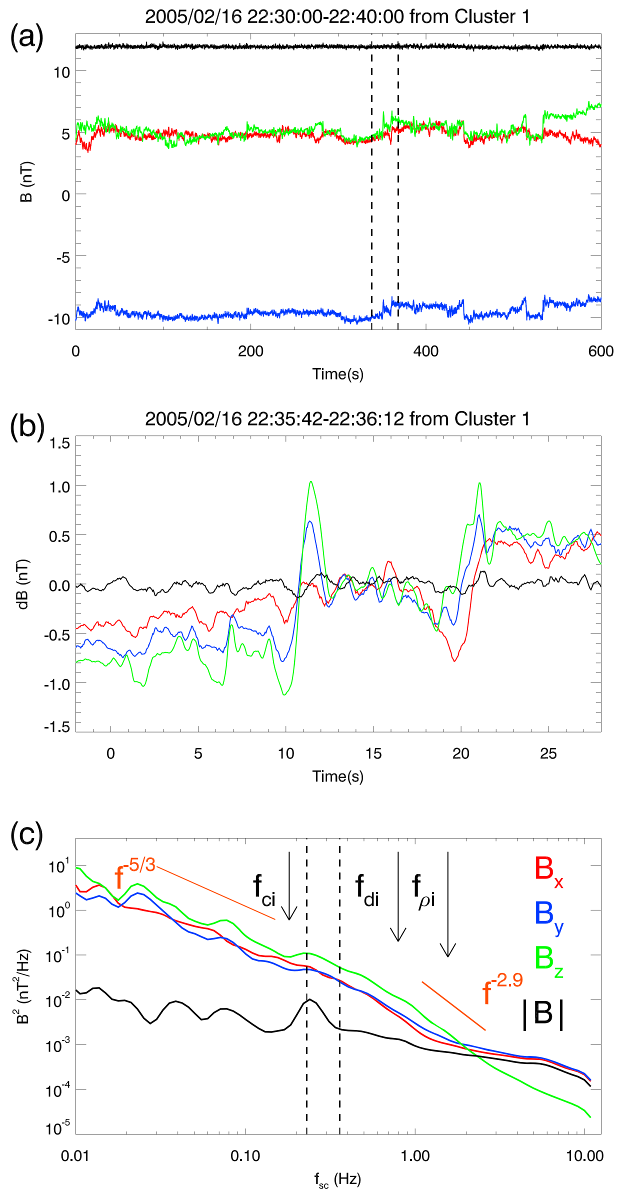

Figure 1. (a) Raw magnetic field time series in the GSE coordinates. Red, blue, and green denote the *x*, *y*, and *z* components of the magnetic field, and black denotes the magnitude. (b) The fluctuations between the two vertical dashed lines magnified where the local mean (time average of 30 s) has been subtracted. The time series have been smoothed with a boxcar average with a width of eight data points (0.32 s) in order to avoid the noise of the FGM instrument at $f \geq 3$ Hz; $t = 0$ s corresponds to 22:35:42 UT. (c) Wavelet power spectra of the magnetic field data in Figure 1a. The vertical lines in Figure 1c denote the range of frequencies where bandpass filtering is performed, while the arrows denote the location of the cyclotron frequency and the "Doppler-shifted" gyroradius and inertial length observed at frequencies $f_{\rho i} = V_{sw}/2\pi\rho_i$ and $f_{di} = V_{sw}/2\pi d_i$, respectively. Orange lines show power law scalings as a guide.

By assuming Taylor's frozen-in condition, the wave number sampled at 0.28 Hz (the center of the enhancement in Figure 2b) has a component along the solar wind flow of $kv_A/\Omega_p \sim 0.38$.

The reconstructed time series of the three components of magnetic field fluctuations are shown in Figure 3. These magnetic field fluctuations are intermittent and consist of wave packets. Here we are able to show that one such wave packet is best described as an Alfvén vortex. The fluctuating magnetic field has very weak compressibility since the parallel component (Figure 3c) is substantially smaller than the two perpendicular components (Figures 3a and 3b). We will focus on an isolated wave packet seen within the zoom boxes of

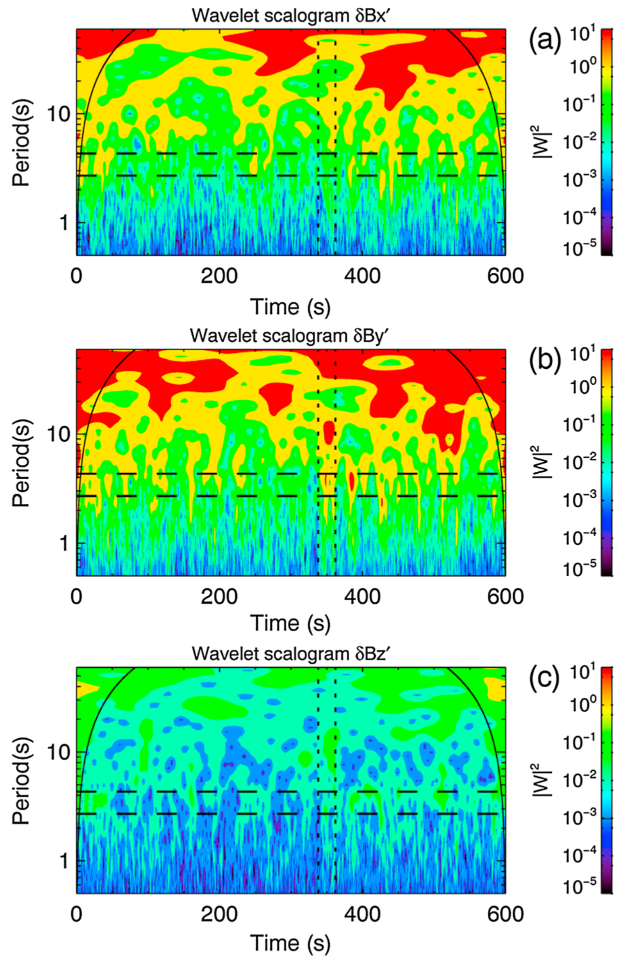

Figure 2. Wavelet scalograms showing the wavelet power for the fluctuations in the three primed coordinates. The solid line denoting the cone of influence region, the dotted lines denoting where we see the wave packet, and the dashed lines denoting the region where we perform frequency filtering.

Figure 3 between $t = 5$ and 15 s. We find that the signals from C1 and C2 in the subinterval are stronger than from the other two satellites.

The spatial scale of the wave packet can be obtained without Taylor's hypothesis by using the phase differencing method [*Dudok de Wit et al.*, 1995; *Walker et al.*, 2004]. It is important to note that this technique can only recover the wave number of the dominant fluctuation at a fixed spacecraft frequency for a wave packet and assumes that it can be described as a plane wave. The difference in phase of the wave packet as observed by two separate spacecraft can be estimated by using a cross correlation to measure the phase shift $\Delta\psi_{i,j}$ between the two signals at spacecraft pairs *i* and *j*. This is related to the wave vector **k** by

$$\Delta\psi_{i,j} = |\mathbf{k}||\mathbf{r_{i,j}}| \cos\theta_{\mathbf{kr}}, \tag{3}$$

where **r** is the separation vector between two spacecraft and $\theta_{\mathbf{kr}}$ is the angle between the wave vector and the spacecraft separation vectors. Essentially, $|\mathbf{k}| \cos\theta_{\mathbf{kr}}$ is the projection of the true wave vector **k** onto the spacecraft separation vector $\mathbf{r_{ij}}$. Cluster's four spacecraft give us the ability to compare the projected wave vector along three separate baselines, thus allowing the determination of the true wave vector. The wave vector projections are related to the true wave vector via

$$\mathbf{k} \cdot \mathbf{A} = \mathbf{k}', \tag{4}$$

where **A** is a 3×3 matrix whose elements are given by three components of the unit vectors of the spacecraft separation vectors corresponding to the three projected wave vectors [*Balikhin et al.*, 2003]. These equations can be solved by inverting **A**. For this wave packet we investigate at a single scale corresponding

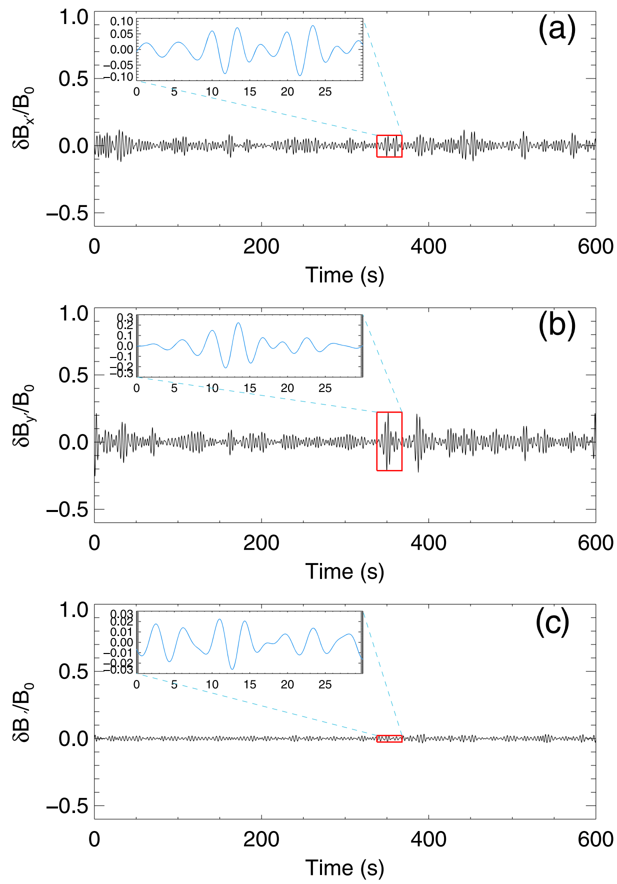

Figure 3. Reconstructed time series of (a) $\delta B_{x'}$, (b) $\delta B_{y'}$, and (c) $\delta B_{z'}$ within 0.23–0.36 Hz frequency range. The wave packet within the two vertical dashed lines, which is one of the strongest in the time interval, will be analyzed thoroughly next. The data are from spacecraft C1.

central frequency of 0.28 Hz where the enhancement is most intense in Figure 2. Other scales of the energetic event yield similar results. The wave vector obtained for this wave packet (from the $\delta B_{y'}$ component) makes a perpendicular angle with the global mean magnetic field $\theta_{\mathbf{kB_0}} = 90.2°$. The wave numbers in the direction parallel and perpendicular to the magnetic field are $k_\parallel \sim 1.8 \times 10^{-5}$ km^{-1}($k_\parallel v_A/\Omega_p \sim 0.0008$) and $k_\perp \sim 5 \times 10^{-3}$ km^{-1}($k_\perp v_A/\Omega_p \sim 0.377$), respectively. The corresponding parallel and perpendicular scales are $\lambda_\parallel \sim 350,000$ km ($9000\rho_i$) and $\lambda_\perp \sim 1200$ km($31.3\rho_i$). The wave packet can be seen in Figure 3 to have approximately 2.5 complete cycles, and therefore, the diameter can be estimated to be $2.5 \times 1200 = 3000$ km ($78.1\rho_i$). By Doppler shifting the frequency to the plasma frame ($\omega_{\mathrm{pla}} = \omega_{\mathrm{sc}} - \mathbf{k} \cdot \mathbf{v}$), a low frequency is obtained of $(0.06 \pm 0.04)\Omega_p$, consistent with previous applications of the k-filtering method at these scales [*Sahraoui et al.*, 2010; *Roberts et al.*, 2013, 2015]. The error is calculated by assuming a 2.5% error on the velocity for the duration of the wave packet of the solar wind. A low plasma frame frequency is indicative of either a slowly moving structure (or one that is advected by the bulk flow) or a linear Kinetic Alfvén wave. The corresponding phase speed estimated from this analysis $V_{\mathrm{ph}\perp} = (1.8 \pm 1.4)$ km/s or $(0.021 \pm 0.016)v_A$. Note that when using this method it is difficult to differentiate between these two scenarios based solely on phase differencing, given the error on the plasma frame frequency. We will now show that the wave packet is best interpreted as an Alfvén vortex.

3. Alfvén Vortex Model

Two types of MHD Alfvén vortex exist: the monopolar one is perfectly aligned with $\mathbf{B_0}$ (θ_{vortex}, the angle between the vortex axis and $\mathbf{B}_0$, is 0°), whereas the dipolar one makes a small angle with $\mathbf{B_0}$ ($\theta_{\mathrm{vortex}} > 0°$).

These vortices are tubular structures quasi-aligned with $\mathbf{B_0}$ and are nonlinear solutions to the incompressible MHD equations. They can be regarded as an MHD counterpart to neutral fluid vortices and have been discussed theoretically by *Petviashvili and Pokhotelov* [1985, 1992].

A dipolar vortex propagates with a small velocity u in the direction of y' relative to the plasma frame. It is convenient to describe the vortex solution using a variable

$$\eta = y' + \alpha z' - ut,\ \ \alpha = \tan(\theta_{\text{vortex}}), \tag{5}$$

where $u = \alpha v_A$ is the speed of the vortex. The full derivation of the vortex can be found in *Petviashvili and Pokhotelov* [1992] and *Alexandrova* [2008], and we simply quote the results expressed with the z' component of the vector potential ($\mathbf{B}_\perp = \nabla A \times \mathbf{e}_{z'}$). The analytical solution reads [*Alexandrova*, 2008]

$$\begin{cases} A = A_0\left(J_0(kr) - J_0(ka)\right) - \frac{2\alpha x'}{kr}\frac{J_1(kr)}{J_0(ka)} + \alpha x', r < a \\ A = A_0 a^2 \frac{\alpha x}{r^2}, r \geq a, \end{cases} \tag{6}$$

where $r = \sqrt{(x')^2 + \eta^2}$, A_0 is a constant amplitude, and $J_n(n = 0, 1)$ is Bessel function of the nth order. Furthermore, a is the vortex radius. For continuity of the solutions, ka must be one of the zeros of Bessel function J_1. Here we will use the third zero of J_1, $ka = 10.17$ to best model the three crests present in the principle fluctuation. The resulting fluctuations within the vortex $r < a$ are then given by

$$\begin{cases} \delta B_{x'} = kA_0 J_0^*(kr)\frac{\eta}{r} + \frac{u}{k\xi}\frac{2}{J_0(ka)}\left[\frac{J_1(kr)}{r} - kJ_1^*(kr)\right]\frac{x'\eta}{r^2}, \\ \\ \delta B_{y'} = -kA_0 J_0^*(ka)\frac{x'}{r} + \frac{u}{k\xi}\frac{2}{J_0(ka)}\left[\frac{J_1(kr)}{r}\eta^2 + kJ_1^*(kr)(x')^2\right]\frac{1}{r^2} - \frac{u}{\xi}. \end{cases} \tag{7}$$

Here the starred J_0 and J_1 denote the derivatives with respect to their arguments, and $\xi = \frac{u}{\alpha}$ is a constant of order unity. For $r \geq a$, we have

$$\begin{cases} \delta B_{x'} = -\frac{2a^2 u}{\xi}\frac{x'\eta}{r^4} \\ \delta B_{y'} = \frac{2a^2 u}{\xi}\left(\frac{(x')^2}{r^4} - \frac{1}{2r^2}\right). \end{cases} \tag{8}$$

The magnetic field fluctuations seen by the spacecraft due to the vortex depend on several parameters, some of which are intrinsic to the vortex and some depend on the path of the spacecraft through the vortex. In the following section we will now describe these parameters of the specific vortex model that we observe.

4. Model Comparison With Solar Wind Data

Figures 4d–4g (solid lines) show magnetic fluctuations on the four Cluster satellites for the same wave packet observed by C1 and shown in Figure 2. One can see that the four satellites observe equivalent signals but not at the same time. These fluctuations will now be compared to the fluctuations from the Alfvén vortex model, described above.

In section 2 we have estimated using four satellites the spatial scale of the fluctuations which we can use here as vortex radius $a = 39.06\rho_i \sim 1500$ km. We have also shown that these fluctuations are convected (in the limits of the error) by the solar wind. Thus, the only free parameters to fit will be the following: a single impact parameter, i.e., the distance of a satellite path to the vortex center at $\eta = 0$, in terms of its radius a; an amplitude A_0; and the inclination of the vortex axis θ_{vortex}. It is important to note that an impact parameter may only be fitted for a single spacecraft; the impact parameters of other spacecraft are constrained by the relative distances to the first spacecraft.

Figure 4a shows the vector potential from equation (6), while Figures 4b and 4c show the resulting magnetic field fluctuations, $\delta B_{x'}$ and $\delta B_{y'}$, from equations (7) and (8), respectively. The arrows denote the trajectories taken by the spacecraft through the vortex. In Figures 4d–4g we show the comparison of the data on four satellites with the Alfvén vortex model fluctuations (dashed lines) measured along the synthetic satellite trajectories shown in Figures 4a–4c. Here we use $A_0 = -1.3B_0\rho_i^2\Omega_p/v_A$ and θ_{vortex}=0.35°. Such small inclination corresponds to a very slow propagation speed of the vortex in the plane perpendicular to $\mathbf{B_0}$, namely, 0.006 v_A. The satellites paths are defined by the solar wind flow in the plane perpendicular to $\mathbf{B}_0$ and by the separations between the satellites, known a priori. The minimal distance from the center of the vortex to the path of C1 is determined to be 0.02a, by varying the impact parameter and comparing the model fluctuations to the data until a good fit is found for the C1 craft. As well, we use $ka = 10.17$ (i.e., the third zero of Bessel function J_1), as mentioned above.

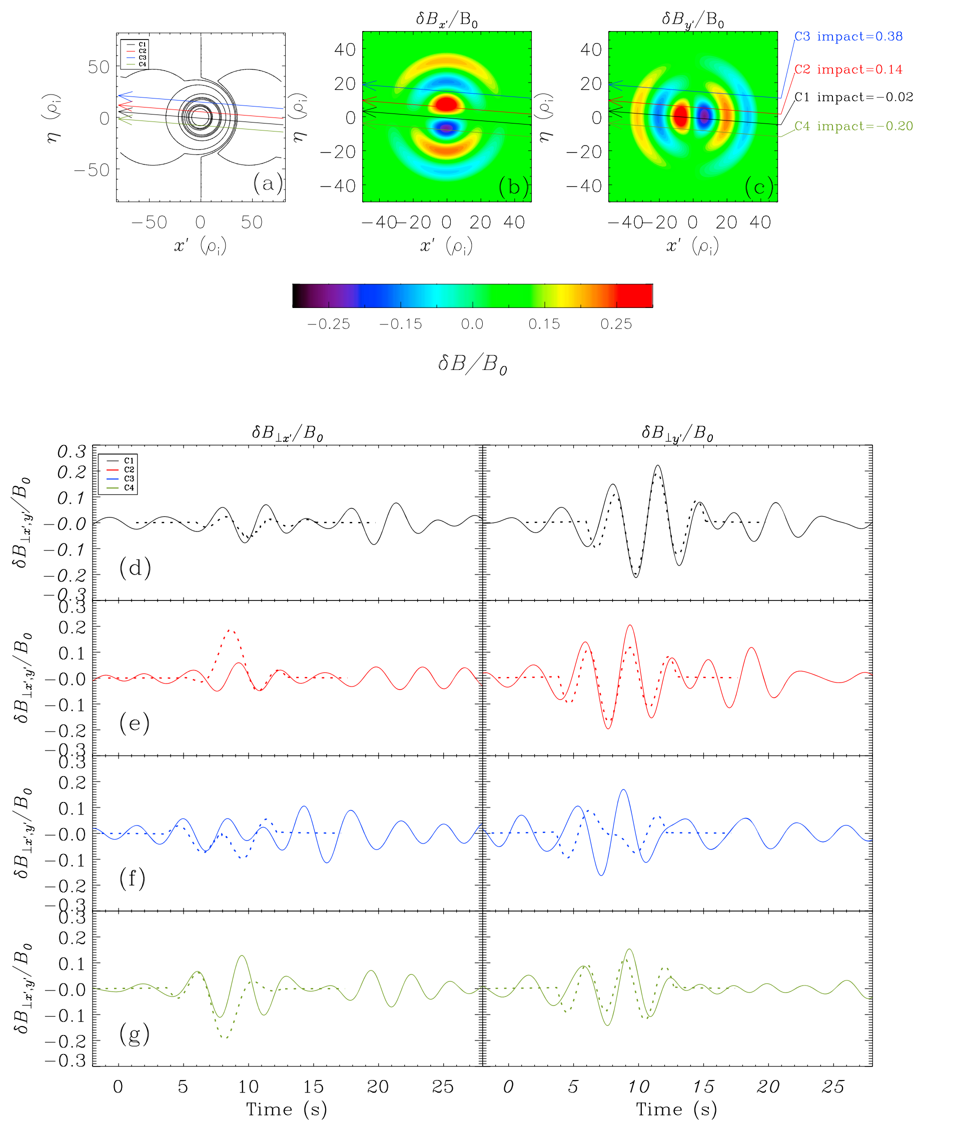

Figure 4. Properties of a quasi-monopolar Alfvén vortex; the axis of the vortex (which is defined as the normal to the $x' - \eta$ plane) makes an angle of 0.35° with $\mathbf{B_0}$. The axes denote distance in units of ρ_i; this vortex propagates at $0.006v_A$ relative to the bulk plasma. (a) The magnetic field lines. (b and c) The perpendicular fluctuations due to the vortex. The arrows denote the paths of the spacecraft through the vortex which give the modeled fluctuations in Figures 4d–4g. Lighter colors refer to positive δB, darker colors refer to negative δB as shown in the color bar. The impact parameters for the various spacecraft are given in units of vortex radius and denote the distance from the vortex axis, passed by $(x', \eta) = 0$. The spacecraft trajectories are denoted by arrows. (d–g) The observed fluctuations (solid line) and the modeled fluctuations (dashed lines) which correspond to the trajectories presented in Figures 4a–4c. The left column shows $\delta B_{x'}$ and the right column shows the $\delta B_{y'}$ with C1 at the top and C4 at the bottom.

A strong agreement for all spacecraft between the measured signals and the modeled signals is seen in Figures 4d–4g for the principal component, which is the $\delta B_{y'}$ component, and to a lesser degree for $\delta B_{x'}$. An interesting result of the fitting is that the C1 craft pass close to the center of the vortex where we would expect a current filament [*Alexandrova*, 2008], which corresponds exactly with the signature of a current seen in Figure 1b. The model shows a stronger agreement for craft C1 and C2 than the other craft. This may be due to the fact that the C1 and C2 craft have smaller impact parameters, making their trajectories closer to the center of the vortex where the amplitudes of the fluctuations are larger. The fitting for $\delta B_{y'}$ for the C3 craft may be less accurate because of the larger impact parameter (see Figure 4c), and the spacecraft pass through a region where the amplitudes are smaller. Outside the vortex radius the analytical solution shows evanescent behavior which is also seen near $t = 2$–7 s; however, near $t = 15$–20 s data show oscillatory behavior

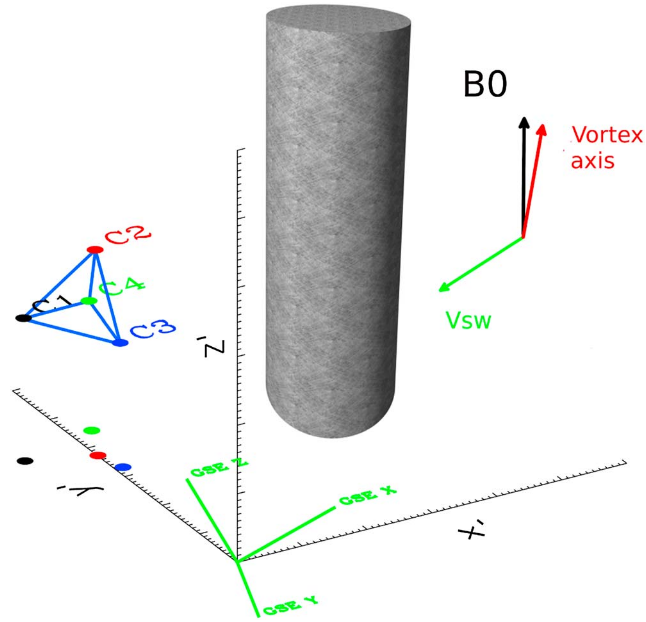

Figure 5. The Cluster spacecraft positions while crossing a tubular structure (Alfvén vortex). The four Cluster satellites are color coded and are located at the vertexes of a tetrahedron. The cylindrical structure denotes the vortex inclined at a small angle to the mean magnetic field, which is directed along the z' direction by construction. The solid colored dots are the projection of the satellites on the $x'Oy'$ plane.

with a smaller amplitude than within the vortex. This is due to the presence of another structure or wave in the vicinity (at $t = 20$ s, Figure 1b) of the studied vortex at $t = 10$ s in Figure 1b. Other discrepancies may also arise either from weak compressibility or that kinetic effects are beginning to play a role at these scales.

Figure 5 depicts the scenario we observe here: an Alfvén vortex is crossed by the Cluster spacecraft. The projections of the spacecraft positions onto the $x'Oy'$ plane are shown by the colored dots.

In our case, the path of the spacecraft makes an angle with the axis of the vortex of 112°, since the magnetic field and solar wind flow form such an angle. Since the displacement of the spacecraft in the z' direction is not constant, this will increase the effective radius seen by the spacecraft. In our case in this coordinate system, the increase of the radius seen by the spacecraft is small (~200 km) compared to the size of the vortex (~3000 km), and the fluctuations do not vary along the z' axis.

The vortex axis is indicated here by a red arrow. From the fitting, we have determined that the angle $\theta_{\text{vortex}} = 0.35°$. Note that this angle is exaggerated in the figure for presentation purposes. Strictly speaking, a monopolar vortex is perfectly aligned with the magnetic field direction and is advected with the solar wind bulk flow. As the angle between the magnetic field direction increases, the vortex becomes a dipolar one, and a quadrupolar structure [*Alexandrova*, 2008, Figure 3] is seen in the perpendicular magnetic field components. However, since the angle is so small, a quadrupolar structure is not seen here. We will use the term "quasi-monopolar" to describe this vortex.

Polarization analysis is another diagnostic technique that can be used to investigate the fluctuations. Here we consider the polarization in the plane perpendicular to the global mean magnetic field $\mathbf{B_0}$. In this plane coherent rotations may signify the presence of coherent structures [*Volwerk et al.*, 1996]. Additionally, the sense of polarization would depend on the path of the spacecraft through the vortex, which could be left/right handed or linear. Figures 6a–6d show this sense of polarization with red (blue) lines denoting right (left)-handed sense of rotation. Note that for the wave interpretation we would expect the polarization to have the same sense for the same wave packet regardless of the point of observation. However, we see that two spacecraft show a mix of both senses of polarization (C1, C2), and the remaining two spacecraft show a strong sense of rotation in opposite directions (C3, C4). These fluctuations are compared to the polarizations predicted from the vortex model in Figures 6e–6h. Good agreement is found between the hodographs obtained from data and the model. A curious feature is that the hodographs vary between spacecraft and are close to being linearly

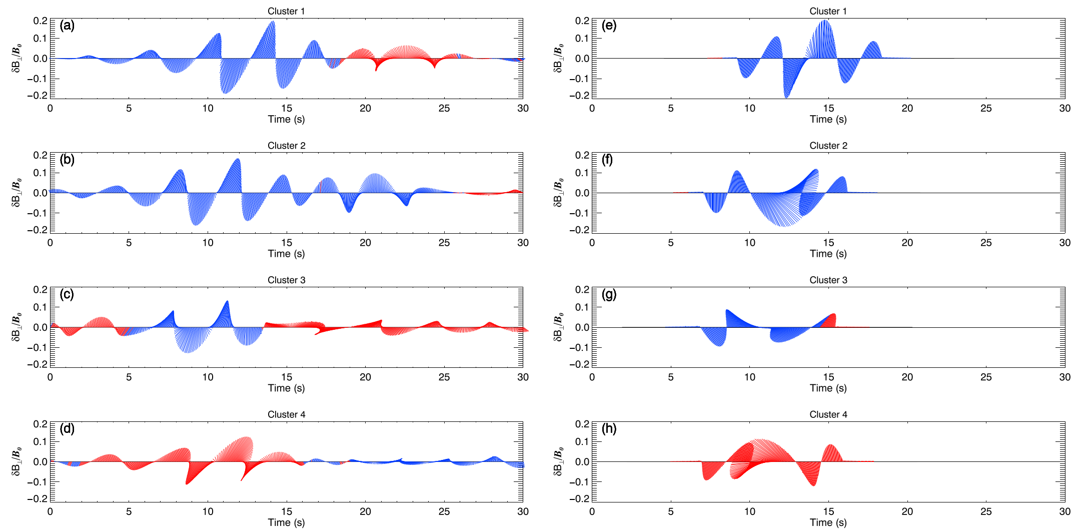

Figure 6. (a–d): Comparison of the polarization observed from the spacecraft ; (e–h) the polarization of the Alfvén vortex model fluctuations, shown by dashed lines in Figures 4d–4g.

polarized for C1 and C2, but polarization is opposite between C3 and C4, which is not expected for a plane wave. The vortex interpretation, however, can explain this rather satisfactorily (see the right panels of Figure 6). An alternative explanation is that the spacecraft were observing two different wave packets. However, this seems unlikely since cross-correlation analysis gives high values for the similarity of the signals between spacecraft, with the largest similarity being 0.96 and the smallest being 0.84 for the $B_{y'}$ components. Thus, the wave packet presented here cannot be described by the wave paradigm, while the Alfvén vortex model reproduces nicely the fluctuations and the polarization for all spacecraft.

5. Conclusion

To summarize, the Cluster spacecraft offer a unique opportunity to study plasma turbulence in three dimensions. We have discussed both linear wave and nonlinear structure paradigms in relation to turbulence. While they are two very different concepts, their measured signatures are very similar and differentiating between both concepts is difficult, emphasizing the need for multipoint measurements. Comparisons between the data obtained from the spacecraft and the Alfvén vortex model show excellent agreement with the real spacecraft distances consistent with their distances in the model. We have also presented a study of the polarization, which shows features that cannot be explained using only linear wave formalism.

In conclusion, we have presented clear evidence of a quasi-monopolar Alfvén vortex in the solar wind. For the wave packet concerned here, a coherent structure aligned with the magnetic field explains the data consistently, while the linear Alfvén wave interpretation alone cannot fully describe the observations. Further research is needed to study whether and how such Alfvén vortices are involved in the turbulent cascading process in the solar wind at 1 AU.

Acknowledgments
All Cluster data are obtained from the ESA Cluster Science Archive: http://www.cosmos.esa.int/web/csa. We thank the FGM and CIS instrument teams and the CSA team. O.R. acknowledges helpful discussions with Khurom Kiyani and Chris Carr. This study is supported in part by the National Natural Science Foundation of China (40904047 and 41174154).

References

Alexandrova, O. (2008), Solar wind vs magnetosheath turbulence and Alfvén vortices, *Nonlinear Processes Geophys.*, *15*, 95–108.

Alexandrova, O., and J. Saur (2008), Alfvén vortices in Saturn's magnetosheath: Cassini observations, *Geophys. Res. Lett.*, *35*, L15102, doi:10.1029/2008GL034411.

Alexandrova, O., A. Mangeney, M. Maksimovic, N. Cornilleau-Wehrlin, J.-M. Bosqued, and M. André (2006), Alfvén vortex filaments observed in magnetosheath downstream of a quasi-perpendicular bow shock, *J. Geophys. Res.*, *111*, A12208, doi:10.1029/2006JA011934.

Alexandrova, O., J. Saur, C. Lacombe, A. Mangeney, J. Mitchell, S. J. Schwartz, and P. Robert (2009), Universality of solar-wind turbulent spectrum from MHD to electron scales, *Phys. Rev. Lett.*, *103*(16), 165003, doi:10.1103/PhysRevLett.103.165003.

Alexandrova, O., C. Lacombe, A. Mangeney, R. Grappin, and M. Maksimovic (2012), Solar wind turbulent spectrum at plasma kinetic scales, *Astrophys. J.*, *760*, 121, doi:10.1088/0004-637X/760/2/121.

Alexandrova, O., S. D. Bale, and C. Lacombe (2013), Comment on "Evidence of a cascade and dissipation of solar-wind turbulence at the electron gyroscale", *Phys. Rev. Lett.*, *111*(14), 149001, doi:10.1103/PhysRevLett.111.149001.

Balikhin, M. A., O. A. Pokhotelov, S. N. Walker, E. Amata, M. Andre, M. Dunlop, and H. S. C. K. Alleyne (2003), Minimum variance free wave identification: Application to Cluster electric field data in the magnetosheath, *Geophys. Res. Lett.*, *30*(10), 1508, doi:10.1029/2003GL016918.

Balogh, A., et al. (2001), The Cluster magnetic field investigation: Overview of in-flight performance and initial results, *Ann. Geophys.*, *19*, 1207–1217, doi:10.5194/angeo-19-1207-2001.

Belcher, J. W. (1971), Alfvénic wave pressures and the solar wind, *Astrophys. J.*, *168*, 509, doi:10.1086/151105.

Bieber, J. W., W. Wanner, and W. H. Matthaeus (1996), Dominant two-dimensional solar wind turbulence with implications for cosmic ray transport, *J. Geophys. Res.*, *101*, 2511–2522, doi:10.1029/95JA02588.

Bruno, R., and V. Carbone (2013), The solar wind as a turbulence laboratory, *Living Rev. Sol. Phys.*, *10*, 2, doi:10.12942/lrsp-2013-2.

Chen, C., T. Horbury, A. A. Schekochihin, R. T. Wicks, O. Alexandrova, and J. Mitchell (2010), Anisotropy of solar wind turbulence between ion and electron scales, *Phys. Rev. Lett.*, *104*, 255002, doi:10.1103/PhysRevLett.104.255002.

Chmyrev, V. M., S. V. Bilichenko, V. I. Pokhotelov, V. A. Marchenko, and V. I. Lazarev (1988), Alfven vortices and related phenomena in the ionosphere and the magnetosphere, *Phys. Scr.*, *38*, 841–854, doi:10.1088/0031-8949/38/6/016.

Décréau, P. M. E., et al. (2001), Early results from the Whisper instrument on Cluster: An overview, *Ann. Geophys.*, *19*, 1241–1258, doi:10.5194/angeo-19-1241-2001.

Dudok de Wit, T., V. V. Krasnosel'skikh, S. D. Bale, M. W. Dunlop, H. Lühr, S. J. Schwartz, and L. J. C. Woolliscroft (1995), Determination of dispersion relations in quasi-stationary plasma turbulence using dual satellite data, *Geophys. Res. Lett.*, *22*, 2653–2656, doi:10.1029/95GL02543.

Escoubet, C. P., R. Schmidt, and M. L. Goldstein (1997), Cluster—Science and mission overview, *Space Sci. Rev.*, *79*, 11–32, doi:10.1023/A:1004923124586.

Goldreich, P., and S. Sridhar (1995), Toward a theory of interstellar turbulence. 2: Strong Alfvenic turbulence, *Astrophys. J.*, *438*, 763–775, doi:10.1086/175121.

Hamilton, K., C. W. Smith, B. J. Vasquez, and R. J. Leamon (2008), Anisotropies and helicities in the solar wind inertial and dissipation ranges at 1 AU, *J. Geophys. Res.*, *113*, A01106, doi:10.1029/2007JA012559.

Hasegawa, H., M. Fujimoto, T.-D. Phan, H. Rème, A. Balogh, M. W. Dunlop, C. Hashimoto, and R. TanDokoro (2004), Transport of solar wind into Earth's magnetosphere through rolled-up Kelvin-Helmholtz vortices, *Nature*, *430*, 755–758, doi:10.1038/nature02799.

He, J., E. Marsch, C.-Y. Tu, S. Yao, and H. Tian (2011), Possible evidence of Alfvén-cyclotron waves in the angle distribution of magnetic helicity of solar wind turbulence, *Astrophys. J.*, *731*, 85, doi:10.1088/0004-637X/731/2/85.

Horbury, T. S., M. Foreman, and S. J. Oughton (2008), Anisotropic scaling of magnetohydrodynamic turbulence, *Phys. Rev. Lett.*, *101*, 175005, doi:10.1103/PhysRevLett.101.175005.

Karimabadi, H., et al. (2013), Coherent structures, intermittent turbulence, and dissipation in high-temperature plasmas, *Phys. Plasmas*, *20*, 012303, doi:10.1063/1.4773205.

Lacombe, C., A. Mangeney, C. C. Harvey, and J. Scudder (1985), Electron plasma waves upstream of the Earth's bow shock, *J. Geophys. Res.*, *90*, 73–94, doi:10.1029/JA090iA01p00073.

Leamon, R. J., C. W. Smith, N. F. Ness, W. H. Matthaeus, and H. K. Wong (1998), Observational constraints on the dynamics of the interplanetary magnetic field dissipation range, *J. Geophys. Res.*, *103*, 4775–4787, doi:10.1029/97JA03394.

Lion, S., O. Alexandrova, and A. Zaslavsky (2016), Coherent events and spectral shape at ion kinetic scales in the fast solar wind turbulence, arXiv:1602.07213 [astro-ph.SR].

Narita, Y., S. P. Gary, S. Saito, K.-H. Glassmeier, and U. Motschmann (2011), Dispersion relation analysis of solar wind turbulence, *Geophys. Res. Lett.*, *38*, L05101, doi:10.1029/2010GL046588.

Orszag, S. A., and C.-M. Tang (1979), Small-scale structure of two-dimensional magnetohydrodynamic turbulence, *J. Fluid Mech.*, *90*, 129–143, doi:10.1017/S002211207900210X.

Petviashvili, V., and O. Pokhotelov (1992), *Solitary Waves in Plasmas and in the Atmosphere*, Gordon and Breach, Philadelphia, Pa.

Petviashvili, V. I., and O. A. Pokhotelov (1985), Dipole Alfvén vortices, *Sov. J. Exp. Theor. Phys. Lett.*, *42*, 54.

Podesta, J. J. (2009), Dependence of solar-wind power spectra on the direction of the local mean magnetic field, *Astrophys. J.*, *698*, 2, doi:10.1088/0004-637X/698/2/986.

Rème, H., et al. (2001), First multispacecraft ion measurements in and near the Earth's magnetosphere with the identical Cluster ion spectrometry (CIS) experiment, *Ann. Geophys.*, *19*, 1303–1354, doi:10.5194/angeo-19-1303-2001.

Roberts, O. W. (2014), Kinetic plasma turbulence at proton gyration scales in the solar wind, PhD thesis, Aberystwyth Univ., U. K.

Roberts, O. W., X. Li, and B. Li (2013), Kinetic plasma turbulence in the fast solar wind measured by Cluster, *Astrophys. J.*, *769*, 58, doi:10.1088/0004-637X/769/1/58.

Roberts, O. W., and X. Li (2015), Evidence of the ion cyclotron resonance at proton kinetic scales in the solar wind, *Astrophys. J.*, *802*, 1, doi:10.1088/0004-637X/802/1/1.

Roberts, O. W., X. Li, and L. Jeska (2015), A statistical study of the solar wind turbulence at ion kinetic scales using the k-filtering technique and Cluster data, *Astrophys. J.*, *802*, 2, doi:10.1088/0004-637X/802/1/2.

Sahraoui, F., M. L. Goldstein, G. Belmont, P. Canu, and L. Rezeau (2010), Three dimensional anisotropic k spectra of turbulence at subproton scales in the solar wind, *Phys. Rev. Lett.*, *105*(13), 131101, doi:10.1103/PhysRevLett.105.131101.

Shebalin, J. V., W. H. Matthaeus, and D. Montgomery (1983), Anisotropy in MHD turbulence due to a mean magnetic field, *J. Plasma Phys.*, *29*, 525–547, doi:10.1017/S0022377800000933.

Shukla, P. K., M. Y. Yu, and R. K. Varma (1985), Drift Alfvén vortices, *Phys. Fluids*, *28*, 6, doi:10.1063/1.864964.

Shukla, P. K., M. Y. Yu, and R. K. Varma (1985a), Formation of kinetic Alfvén vortices, *Phys. Rev. A*, *109*, 7, doi:10.1016/0375-9601(85)90183-5.

Siscoe, G. L., L. Davis Jr., P. J. Coleman Jr., E. J. Smith, and D. E. Jones (1968), Power spectra and discontinuities of the interplanetary magnetic field: Mariner 4, *J. Geophys. Res.*, *73*, 61–82, doi:10.1029/JA073i001p00061.

Smith, C. W., W. H. Matthaeus, G. P. Zank, N. F. Ness, S. Oughton, and J. D. Richardson (2001), Heating of the low-latitude solar wind by dissipation of turbulent magnetic fluctuations, *J. Geophys. Res.*, *106*, 8253–8272, doi:10.1029/2000JA000366.

Smith, C. W., K. Hamilton, B. J. Vasquez, and R. J. Leamon (2006), Dependence of the dissipation range spectrum of interplanetary magnetic fluctuations on the rate of energy cascade, *Astrophys. J. Lett.*, *645*, L85–L88, doi:10.1086/506151.

Sundkvist, D., V. Krasnoselskikh, P. K. Shukla, A. Vaivads, M. André, S. Buchert, and H. Rème (2005), In situ multi-satellite detection of coherent vortices as a manifestation of Alfvénic turbulence, *Nature*, *436*, 825–828, doi:10.1038/nature03931.

Sundkvist, D., and S. D Bale (2008), Characteristic parameters of drift vortices coupled to Alfvén waves in and inhomogeneous space plasma, *Phys. Rev. Lett.*, *101*, 065001, doi:10.1103/PhysRevLett.101.065001.

Torrence, C., and G. P. Compo (1998), A practical guide to wavelet analysis, *Bull. Am. Meteorol. Soc.*, *79*, 61–78, doi:10.1175/1520-0477(1998)079<0061:APGTWA>2.0.CO;2.

Tu, C.-Y., and E. Marsch (1995), MHD structures, waves and turbulence in the solar wind: Observations and theories, *Space Sci. Rev.*, *73*, 1–210, doi:10.1007/BF00748891.

Vasquez, B. J., V. I. Abramenko, D. K. Haggerty, and C. W. Smith (2007), Numerous small magnetic field discontinuities of Bartels rotation 2286 and the potential role of Alfvénic turbulence, *J. Geophys. Res.*, *112*, A11102, doi:10.1029/2007JA012504.

Verkhoglyadova, O. P., B. Dasgupta, and B. T. Tsurutani (2003), Model for vortex turbulence with discontinuities in the solar wind, *Nonlinear Processes Geophys.*, *10*, 335–343.

Volwerk, M., P. Louarn, T. Chust, A. Roux, H. de Feraudy, and B. Holback (1996), Solitary kinetic Alfvén waves: A study of the Poynting flux, *J. Geophys. Res.*, *101*, 13,335–13,344, doi:10.1029/96JA00166.

Walker, S., F. Sahraoui, M. Balikhin, G. Belmont, J. Pinçon, L. Rezeau, H. Alleyne, N. Cornilleau-Wehrlin, and M. André (2004), A comparison of wave mode identification techniques, *Ann. Geophys.*, *22*, 3021–3032, doi:10.5194/angeo-22-3021-2004.

Wicks, R. T., T. S. Horbury, C. H. K. Chen, and A. A. Schekochihin (2010), Power and spectral index anisotropy of the entire inertial range of turbulence in the fast solar wind, *Mon. Not. R. Astron. Soc. Lett.*, *407*, L31–L35, doi:10.1111/j.1745-3933.2010.00898.x.